Structural reversibility of a ternary $CuO–ZnO–Al_2O_3$ *ex* hydrotalcite-containing material during wet Pd impregnation

I. Melián-Cabrera, M. López Granados, and J.L.G. Fierro *

Instituto de Catálisis y Petroleoquímica (CSIC), Campus UAM, Cantoblanco 28049, Madrid, Spain

Received 23 April 2002; accepted 15 August 2002

A Cu–Zn–Al precursor was synthesized by coprecipitation of the corresponding cations with sodium carbonate at constant pH and temperature. $CuO–ZnO–Al_2O_3$ composite oxide support was obtained by calcination (673 K) of the Cu–Zn–Al precursor. Two palladium-modified $CuO–ZnO–Al_2O_3$ samples were prepared by impregnation of the mixed-oxide support and further calcination (673 K). The presence of remaining CO_3^{2-} anions in the $CuO–ZnO–Al_2O_3$ mixed oxide, as a result of incomplete Cu–Zn hydrotalcite phase decomposition, and the hydrothermal-like treatment during the Pd impregnation step, allow the partial reconstruction of the Cu–Zn hydrotalcite-type structure (memory effect). In addition, an enhancement in the CuO crystallinity was obtained for the Pd-modified oxides. A detailed characterization revealed that the hydrotalcite restoration enhances the crystallinity of the copper oxide as a consequence of a crystalline rearrangement of this oxidic phase.

KEY WORDS: rehydration; hydrotalcite reconstruction; Pd-modifed materials; methanol synthesis catalysts.

1. Introduction

The conventional Cu–Zn–Al mixed-oxide catalytic material, which is used for the synthesis of methanol from $CO/CO_2/H_2$ mixtures (synthesis gas), is obtained from decomposition of a hydroxycarbonate precursor. This classical hydroxycarbonate route leads to the formation of several mixed-metal hydroxycarbonates such as aurichalcite, $(Cu,Zn)_5(CO_3)_2(OH)_6$, zincian–malachite (or rosasite), $(Cu,Zn)_2(OH)_2CO_3$, and a Cu–Zn hydrotalcite-like phase $(Cu,Zn)_6Al_2(OH)_{16}\ CO_3{\cdot}4H_2O$, which all decompose to give well-dispersed oxidic phases [1–3]. The Cu–Zn hydrotalcite-like phase is a very important component of the mixed-phase-containing precursor for methanol synthesis catalysts. This material belongs to the so-called hydrotalcite-like compounds (HTlcs), which are a family of materials consisting of layered double hydroxides of general formula: $[M^{II}_{1-x}M^{III}_x(OH)_2]^{x+}(A^{n-})_{x/n}{\cdot}mH_2O$, where M^{II} and M^{III} are di- and trivalent metal cations that occupy octahedral positions in brucite-like layers, A^{n-} is the interlayer anion, m the number of interlayer water molecules and x the atomic ratio $M^{III}/(M^{II}+M^{III})$ [4].

The conventional $CuO–ZnO–Al_2O_3$ mixed-oxide catalyst, obtained from the hydroxycarbonate route, has achieved excellent performance in industrial methanol synthesis. However, there have been many claims that the catalyst performance can be enhanced by increasing the dispersion of the copper phase as well as by adding a promoter other than a mere copper dispersion enhancing agent [5,6]. One way to achieve this goal is the incorporation of palladium within the $CuO–ZnO–Al_2O_3$ material. Palladium is an excellent candidate to split the H−H bond, and the resulting H atoms subsequently spread over the neighboring phases through a hydrogen spillover mechanism [7–10]. This process leads to the surface of the catalyst being in a more reduced state, a situation that may further facilitate surface hydrogenation reactions.

A standard procedure to introduce palladium is the so-called wet impregnation technique. An excess of a solution containing the palladium precursor is contacted with the support oxide and the excess solvent is then removed by drying. It should be noted, however, that if the preparation of the Pd-supported oxide is performed by aqueous impregnation, some partially decarbonated oxides could regenerate their initial hydrotalcite structure (memory effect [11,12]) by hydration during the metal impregnation step. Such rehydrated hydrotalcite-containing oxides must be calcined again before they can be used as modified methanol synthesis catalysts. The resulting hydration/recalcination cycle may affect the dispersion of the oxidic phases and hence the catalyst activity. Recent studies [13] on hydrotalcite reconstruction of mixed metal oxides derived from hydrotalcite decomposition show that this phenomenon is more complex than previously thought [11,12].

Given the findings outlined above, gaining an understanding of this process, which could take place simultaneously during the aqueous palladium impregnation of $CuO–ZnO–Al_2O_3$ mixed oxide, is of vital importance in explaining the further catalytic activity of the modified materials. Considering the fact that the rehydration

* To whom correspondence should be addressed.
E-mail: jlgfierro@icp.csic.es

1011-372X/02/1200-0153/0

phenomenon of such ternary CuO–ZnO–Al_2O_3 oxides has scarcely been studied, the aim of this work was to study the effect of the hydration/recalcination cycle on the dispersion of the final CuO phase during the aqueous impregnation of Pd onto the CuO–ZnO–Al_2O_3 composite material.

2. Experimental

2.1. Material preparation

The CZA precursor (Cu:Zn:Al = 55:30:15 atomic ratio) was prepared by coprecipitation at constant pH (*ca.* 7) and constant temperature (343 K). A solution containing metal nitrates ($[Cu^{2+}]+[Zn^{2+}]+[Al^{3+}]=1.0$ M) and a sodium carbonate solution (1.1 M) were simultaneously added to a reaction vessel containing a small amount of deionized water (18 MΩ/cm, as supplied by Millipore deionizer). All the reagents were of analytical grade (Aldrich). The suspension was continuously stirred and kept at the desired pH by adjusting the relative flow rates of the two solutions. The final suspension was aged under stirring (343 K for 4 h) and cooled down to room temperature overnight. The precipitate was filtered off and repeatedly washed with sufficient deionized water to ensure that the sodium content in the solid was lower than 0.05 wt%. The solid was dried overnight at 393 K (precursor) and calcined in air at 673 K for 4 h (catalyst). The resulting powder (calcined CZA) was used as the starting material for the preparation of the palladium-modified samples.

Two Pd-containing materials were prepared by impregnation of the base CZA with an aqueous $Pd(NO_3)_2$ (Alfa Aesar, reagent grade) solution of appropriate concentration to obtain a Pd loading of 4.0 and 9.0 wt%, respectively. The method involved adding 4.0 g of CZA powder to 100 ml of palladium nitrate solution at 353 K. The solution was then evaporated to dryness under vacuum using a rotary evaporator (2–3 h) and the resulting powder was calcined once again (673 K for 4 h). The base material was initially outgassed at room temperature under vacuum, before the addition of the $Pd(NO_3)_2$ solution. The samples are denoted as XPd/CZA, where X is the nominal loading of palladium (wt%) in the calcined material and CZA represents the CuO–ZnO–Al_2O_3 mixed oxide.

2.2. Sample characterisation

Thermogravimetric curves (TG) were recorded with a Perkin-Elmer TGS-2 analyzer. The sample holder was loaded with 5–10 mg of specimen and the decomposition of the precursor was monitored in an air flow of 40 ml/min and at a heating rate of 4 K/min. Evolved gas analysis (EGA-MS) of the precursor decomposition was performed by mass spectrometry. Samples of 10–20 mg were placed in a U-shaped quartz reactor incorporated within a flow system. The reactor exit line was connected to a Baltzer Prisma™ quadrupole mass spectrometer QMS 200. A mixture of 21% O_2 in Ar was introduced at a rate of 40 ml/min and the temperature was increased at 4 K/min while the composition of evolved gases was continuously monitored. The experimental errors for the TGA and EGA experiments were 1.0 and 2.5%, respectively.

Powder X-ray diffraction (XRD) patterns were recorded on a computerized Seifert 3000 X-ray diffractometer using Cu K_α radiation, a PW 2200 goniometer (Bragg–Brentano $\theta/2\theta$), a bent graphite monochromator and an automatic slit. All the samples were scanned between $10^\circ < 2\theta < 75^\circ$ in the step mode (0.02°, 2 s). The mean crystalline size (D) of CuO was determined from the line broadening of the (111) ($2\theta = 38.77^\circ$) diffraction line using the Scherrer equation after correction for instrumental broadening, $D = K\lambda/\beta\cos\theta$ with $K = 0.9$. Owing to overlapping of the CuO(111) and Cu(200) reflections in the range $37^\circ < 2\theta < 41^\circ$, it was necessary to decompose the XRD profile into two contributions by applying curve-fitting procedures.

The specific area of the calcined samples was calculated from the N_2 adsorption isotherms at 77 K, which were determined on an ASAP 2010 apparatus using the BET method and a value of 0.1620 nm^2 for the cross section of a physically adsorbed N_2 molecule. The samples were evacuated at 413 K overnight prior to N_2 dosage.

3. Results and discussion

3.1. Characterization of the CZA precursor

The XRD pattern of the CZA precursor is presented in figure 1(A). For the sake of comparison, the JCPDS files for several reference compounds are also included in the lower part of this figure. The typical pattern of the Cu–Zn hydrotalcite-like structure [$Cu_2Zn_4Al_2(OH)_{16}CO_3{\cdot}4H_2O$], JPCDS 38-487 [14], can clearly be seen in the base CZA precursor. The remaining diffraction peaks have been assigned to a rosasite phase [$(Cu,Zn)_2CO_3(OH)_2$], JCPDS 36-1475 [15]. Although the intensities of the two peaks at $2\theta \approx 32^\circ$ do not correspond to the intensity reported in any of the rosasite JCPDS files, our assignment is based on other literature work [16,17]. In addition, it must be considered that the rosasite phase is a zincian–malachite that can be described as a solid solution in which the Cu/Zn ratio can influence the intensity of the diffraction peaks of the pattern.

Figure 2 shows the thermal decomposition of the CZA precursor studied by two methods: TG analysis (figure 2(A)) and EGA-MS analysis, which involved monitoring the H_2O and CO_2 evolution by detection of

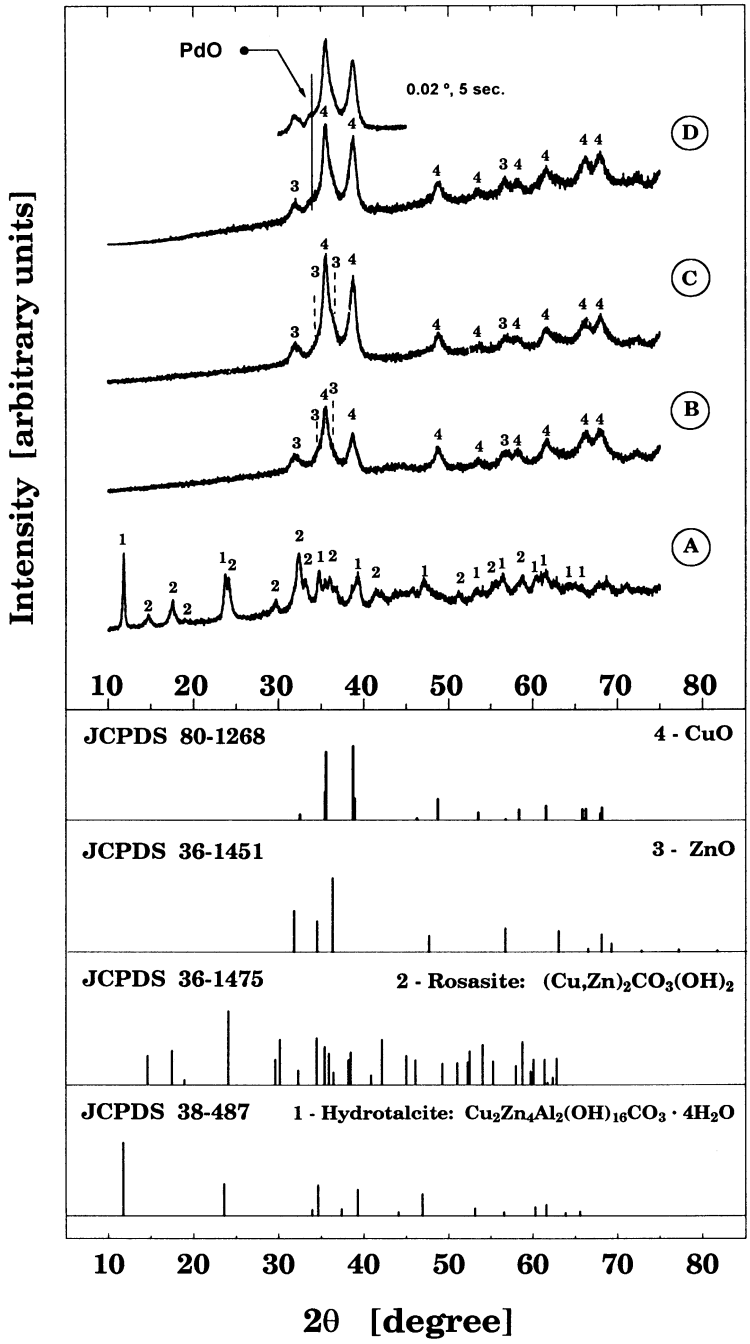

Figure 1. X-ray powder diffraction profiles for: (A) CZA precursor, (B) CZA mixed oxide: CuO–ZnO–Al_2O_3, (C) 4Pd/CZA and (D) 10Pd/CZA calcined samples.

fragments at $m/z = 18$ and 44 with a quadrupole mass spectrometer (solid line in figure 2(B)). For the sake of clarity, the derivative curve of the TG trace is also included in figure 2(A) (dashed line).

There is correspondence between the processes observed by TG analysis and by MS detection. The precursor undergoes four weight-loss processes upon heating under a flow of air. The first weight loss is associated with removal of water of crystallization present in the Cu–Zn hydrotalcite-like structure, and this is clearly visible in the derivative TGA peak at *ca.* 440 K. A second process, defined by the broad peak at 570 K, is due to H_2O and CO_2 co-evolution during decomposition of the hydrotalcite and rosasite phases. Elimination of structural hydroxyl groups from both phases resulted in the formation of H_2O, but the evolution of CO_2 is only due to the decomposition of the rosasite. Finally, the hydrotalcite carbonate groups decompose in the next two weight-loss processes, which occur in the range 700–900 K. This fact indicates that at temperatures below 673 K (the calcination temperature) the hydrotalcite CO_3^{2-} units will remain occluded

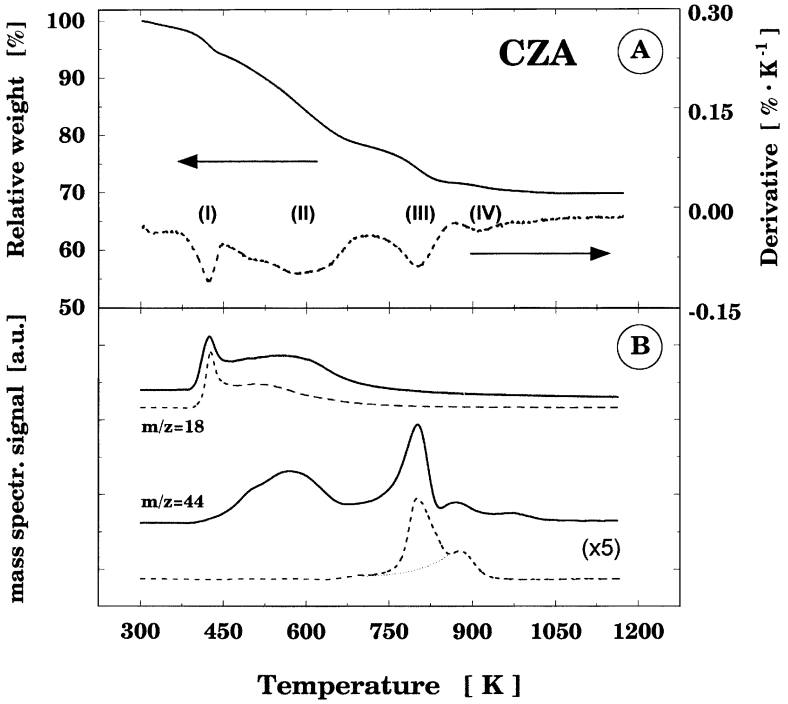

Figure 2. (A) Thermogravimetric (TGA) curve of the CZA precursor. The dashed line corresponds to the derivative curve. (B) Mass spectrometry traces of H_2O ($m/z = 18$) and CO_2 ($m/z = 44$) evolved for the CZA precursor (solid lines) and $Cu_2Zn_4Al_2(OH)_{16}CO_3{\cdot}xH_2O$ hydrotalcite as a reference compound (dashed lines).

in the solid. The assignment of this peak to the decomposition of CO_3^{2-} groups from the hydrotalcite is not only based on data reported in the literature [4,18–20] but also on TG and EGA-MS analyzes of a $Cu_2Zn_4Al_2(OH)_{16}CO_3{\cdot}4H_2O$ hydrotalcite-like compound (labeled as HT Cu–Zn) prepared in our laboratory according to the method described elsewhere [18]. The characterization of this material by XRD will be reported below for the sake of clarity. The analysis showed (see dashed lines in figure 2(B)) H_2O evolution at 440 K (dehydration) and 550 K (dehydroxylation), followed by CO_2 formation between 750 and 900 K resulting from carbonate decomposition.

3.1.1. Characterization of Cu–Zn hydrotalcite by XRD

This material, a component of the CZA precursor, became an essential reference compound in the interpretation of the EGA-MS analysis of the CZA catalyst precursor. The XRD pattern of the as-synthesized HTCu-Zn material (figure 3(A)) shows a hydrotalcite structure (JPCDS 38-487) [14], exhibiting sharp and symmetric reflections of the basal (003), (006), and (009) planes, and broad and slightly asymmetric reflections for the non-basal (012), (015), and (018) planes. The (009) and (012) reflections overlap in the range of $32^\circ < 2\theta < 38^\circ$ and the two hydrotalcite distinctive reflections of the (110) and (113) planes can be clearly distinguished around $2\theta = 60^\circ$. The cell parameters a and c have been also calculated and compared with those reported in the literature. The parameter a of the

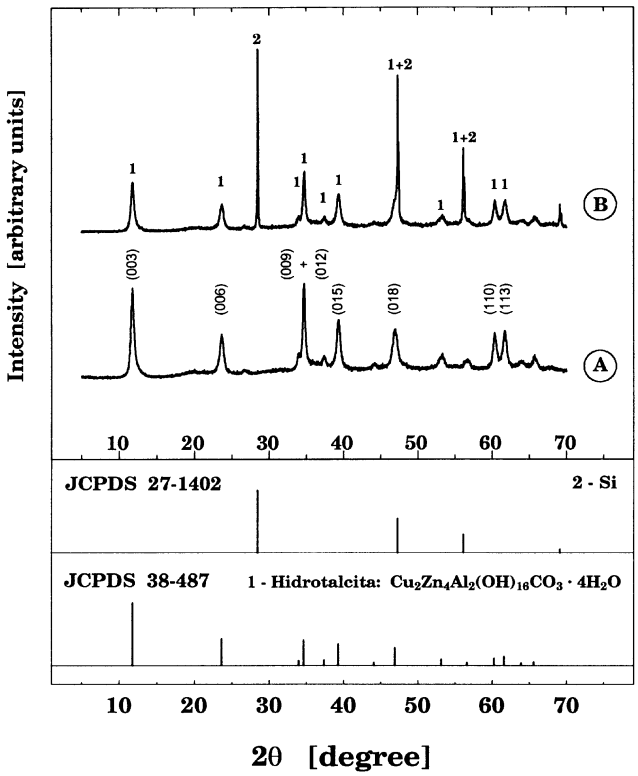

Figure 3. X-ray powder diffraction profiles for: (A) HT Cu–Zn [$Cu_2Zn_4Al_2(OH)_{16}CO_3{\cdot}xH_2O$] and (B) HT Cu–Zn mixed with pure Si as reference.

Table 1
Lattice parameters (nm) for the Cu–Zn hydrotalcite-like compound prepared (HTCu–Zn).

Sample	Formula	a [c]	c_R [d]	c_R [e]
HTCu–Zn	$Cu_2Zn_4Al_2(OH)_{16}CO_3{\cdot}xH_2O$	0.3064	2.2473	2.2511
HTMg [a]	$Mg_6Al_2(OH)_{16}CO_3{\cdot}4H_2O$	0.3054	2.2810	–
HTMg [b]	$Mg_{0.64}Al_{0.36}(OH)_2\ (CO_3)_{0.18}{\cdot}0.46H_2O$	0.3046	2.2772	–

[a] Taken from Ref. [4].
[b] Taken from Ref. [21].
[c] $a = 2{\cdot}d(110)$. The reflection (110) was corrected by Si $d(400) = 0.13579$, JCPDS 27-1402.
[d] $c_R = 3{\cdot}d(003)$, assuming 3R polytypism for this hydrotalcite. Reflection (003) was corrected by Si $d(110) = 0.31379$, JCPDS 27-1402.
[e] For broadened peaks the expression $c_R = 3/2[d(003) + 2{\cdot}d(006)]$ is recommended [22,23].

layered structure corresponds to the average cation–cation distance within the layers and can be calculated as $a = 2{\cdot}d(110)$ [4]. The c parameter, which is related to the thickness of the brucite-like layer and the interlayer distance (see the top of figure 5), is commonly calculated as $c = 3{\cdot}d(003)$, assuming a 3R polytypism for the hydrotalcite [21], *i.e.*, the unit cell covers three sheets with rhombohedral symmetry. The observed interplanar d-spacings used for the computations of the cell parameters were corrected using pure silicon as an external standard (see figure 3(B)). The values were estimated and given in table 1.

The parameter a is quite similar to those reported for various Mg-Al hydrotalcites [4,21], whereas parameter c appears to be slightly lower than those reported. The difference could be related to the assumption that $c = 3{\cdot}d(003)$, since this computation is only applicable if the (00l) reflections are sharp. A closer observation of the XRD profile (figure 3(B)) shows that the (00l) reflections are somewhat broad. It has been proposed for broad peaks that c can be better determined by averaging the position of the diffraction peaks corresponding to planes (003) and (006) according to the formula $c = 3/2[d(003) + 2{\cdot}d(006)]$ [22,23]. The new value obtained (2.2511 nm) was higher than initially estimated but it is still lower than those reported for Mg-Al hydrotalcites. Such a shorter difference in parameter c can be ascribed to differences in the degree of hydration between the samples.

3.2. Characterization of the calcined samples

The CZA precursor was calcined in air (673 K) to give the starting material for the subsequent Pd impregnation. The temperature of calcination was selected as 673 K on the basis of the TGA and EGA-MS studies, which indicated an almost complete decomposition of the precursor at this temperature. Higher calcination temperatures, as required to decompose the remaining CO_3^{2-}, were not used as they are close to the higher limit allowed to minimize thermal sintering of the CuO phase. Such sintering has a detrimental effect on the catalytic activity for the methanol synthesis reaction.

3.2.1. Cu–Zn–Al mixed oxide (CZA)

The XRD pattern of the calcined CZA material is shown in figure 1(B). Although the most intense diffraction lines at $30^\circ < 2\theta < 40^\circ$ are overlapped, the peaks could be assigned to the CuO (JCPDS 80-1268 [24]) and ZnO (JCPDS 36-1451 [25]) phases. The broad XRD peaks indicate that the Cu and Zn oxides are ill-defined crystalline phases. Similar results have been reported by different authors for other CuO–ZnO-based composite materials prepared under similar conditions [26,27]. The coprecipitation results in the formation of Cu–Zn mixed phases like rosasite and a Cu–Zn hydrotalcite-like phase in which the Cu and Zn are atomically dispersed in a hydroxycarbonate matrix. When these phases are calcined, CuO and ZnO are formed with a smaller crystal size than those derived from single phases like malachite (pure Cu–hydroxocarbonate) and hydrozincite (pure Zn–hydroxocarbonate) [1–3]. Moreover, a small amount of Cu(II) cations (*ca.* 2 at%) can be dissolved in the ZnO lattice [28], a situation that can clearly introduce some disorder into the framework, as evidenced by the broad XRD peaks for the ZnO phase. The nature and precise arrangement of the CO_3^{2-} units remaining in the mixed oxide—a consequence of incomplete Cu–Zn hydrotalcite decomposition—have not been examined in detail in the literature. In fact, no Cu–Zn carbonate is detected by XRD, which indicates that the phase must be amorphous. However, it is believed that the thermally-induced changes in the hydrotalcite-like compounds take place through a topotactic decomposition of the brucite-like layers, giving an oxycarbonate in which the metal–oxygen framework remains essentially intact and the carbonate anions are still retained in the interlayer region.

3.2.2. Pd-modified calcined samples (Pd/CZA)

The impregnation with palladium was carried out on the $CuO–ZnO–Al_2O_3$ mixed-oxide support described above. XRD patterns of the calcined Pd-containing samples are represented in figures 1(C) (4Pd/CZA) and 1(D) (10Pd/CZA). At first glance, these profiles seem to be very similar to that of the calcined CZA sample.

Table 2
BET specific area and CuO crystal size for CZA and Pd-modified calcined samples.

Sample	BET area (m^2/g)	XRD crystal size D_{CuO} (nm)
CZA	39.5	8.1
4Pd/CZA	31.8	10.8
10Pd/CZA	30.1	11.0

Closer examination, however, shows that the CuO peaks are sharper for the modified materials in comparison to CZA while the ZnO peaks remain essentially unaffected. Since the width of an XRD peak is related to the size of the crystallites, it can be concluded that the sharper the CuO diffraction peaks, the bigger the average size of CuO particles of the size distribution. The crystallite size of the CuO phase can be quantitatively estimated by the line broadening of the (111) diffraction line at $2\theta \approx 38.77^\circ$ by applying the Scherrer equation (see section 2). The values are listed in table 2 and indicate that the CuO crystal size for the calcined Pd-containing samples is larger than for the CZA sample. In the case of the 10Pd/CZA sample, a weak peak at $2\theta \approx 33.84^\circ$, which is partially overlapped with CuO and ZnO contributions, appeared upon using a slower scanning rate between $30^\circ < 2\theta < 45^\circ$ (see top profile in figure 1). This feature points to incipient formation of PdO crystallites. The absence of clear evidence of PdO in 4Pd/CZA indicates that the PdO phase is rather well dispersed over the surface of the calcined CZA. The PdO crystallites are detected only for higher loadings.

The specific BET areas of the calcined materials are given in table 2. A marked decrease in the specific area is observed when Pd is added to the base-calcined CZA. Furthermore, the decrease in BET area for the two Pd-modified samples is almost equal. The increase in the average CuO crystal size agrees with the lower BET area found for the Pd-modified samples, a fact that might be caused by the exposure to water during the palladium impregnation step.

3.3. Rehydration of the base-calcined CZA sample

In the previous section, it was suggested that the enhancement in CuO crystal size in the Pd-modified materials might be caused by the exposure to water during the impregnation with a palladium solution. In an attempt to confirm this idea, a blank experiment was carried out on the calcined starting material (CZA), whereby the calcined sample was subjected to the aforementioned aqueous impregnation procedure without the palladium precursor present in the aqueous solution. The solid obtained in this way was dried again at 393 K and recalcined at 673 K.

In figure 4 the XRD pattern of the calcined CZA base support (figure 4(A)) is compared with the materials obtained by rehydration (rehydrated CZA) (figure 4(B)) and after calcination (recalcined CZA) (figure 4(C)). The rehydrated CZA material displays the characteristic peaks due to the CuO and ZnO phases as well as the typical pattern of the Cu–Zn hydrotalcite-like structure, which proves that the hydrotalcite phase became partially regenerated. The presence of the remaining CO_3^{2-} anions in the CZA mixed oxide and the thermal treatment with water in the rotary evaporator (*i.e.*, a hydrothermal-like treatment) allow the partial reconstruction of the initial lamellar Cu–Zn hydrotalcite-type structure (memory effect). It is believed that the hydrotalcite regeneration is facilitated by the fact that the thermal hydrotalcite decomposition occurs through a topotactic process, where the CO_3^{2-} anions are still retained in the interlayer region of the oxycarbonate and the metal–oxygen framework remains essentially intact. In fact, recent studies [29,30] suggest that the reformation occurs *via* a retrotopotactic transformation, *i.e.*, a reverse topotactic transformation. A structural model about the decomposition–reconstruction mechanism (structural reversibility) is illustrated in figure 5. After interlayer water removal, additional water is formed by dehydroxylation of neighboring OH groups within the brucite-like layer and then from OH groups of contiguous layers, causing the collapse of the lamellar structure. Dehydroxylation of the sample creates oxygen vacancies in the structure but without changing the close-packed cubic lattice of anions (O^{2-}). Therefore, the initial hydrotalcite structure, as shown in the top of the figure 5, partially collapses upon heating and an oxycarbonate is formed (bottom). It can also be noticed that Al^{3+} cations change their coordination from octahedral to tetrahedral, while the coordination of bivalent cations remains unchanged. This fact is supported by ^{27}Al MAS-NMR studies which proved that only Al^{3+} cations change from octahedral to tetrahedral configuration [31,32]. In addition, the increase of the calcination temperature suppresses the memory effect of such materials. First, the residual carbonate is evacuated and, second, high temperatures facilitate the solid-state transformation of Al^{3+} cations to tetrahedral positions, to form the spinel structure. Therefore, the recrystallization does not take place since both M^{2+}/Al^{3+} cations in octahedral sites are required. The reverse process, also reflected in figure 5, is facilitated by treatment of the carbonate-containing oxides with water and temperature (hydrothermal-like treatment). It appears evident that the reverse process becomes easier by applying carbonate-containing aqueous solutions, or also with anions other than carbonates.

Proceeding with the analysis of the derived materials, the CuO diffraction peaks for rehydrated CZA are narrower in comparison to those for calcined CZA, whereas ZnO does not show an enhancement in the

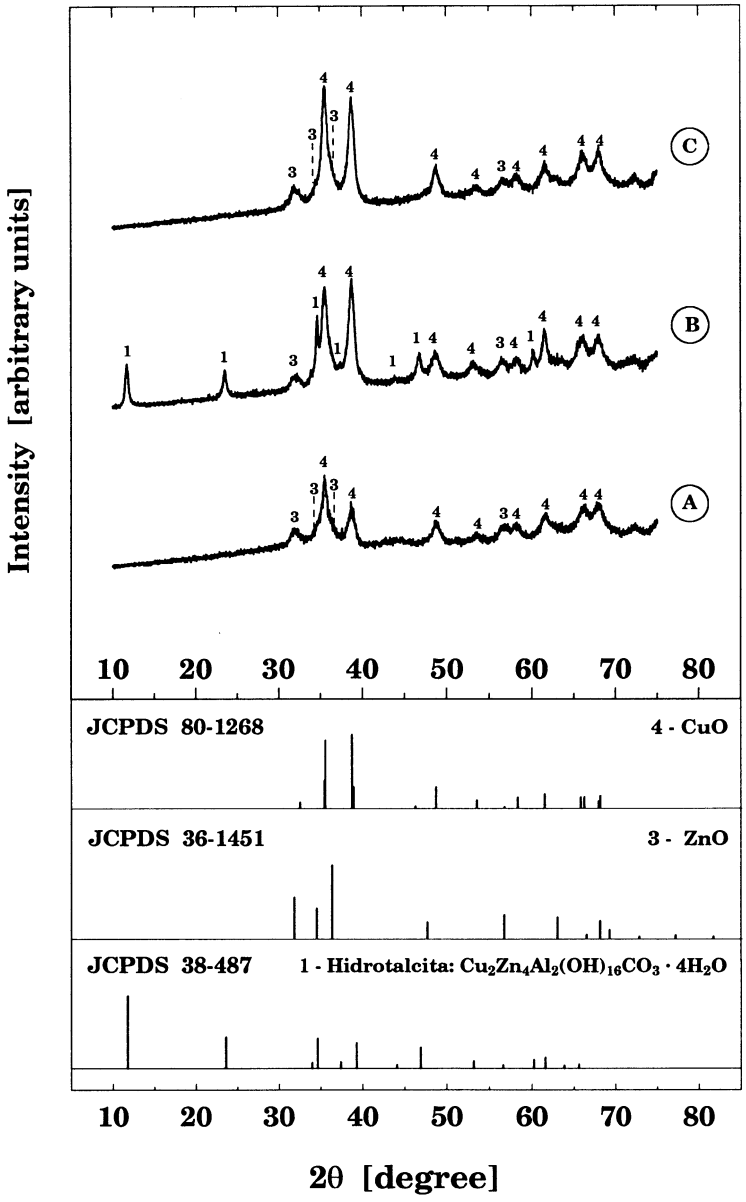

Figure 4. X-ray powder diffraction profiles for: (A) calcined-CZA, (B) rehydrated-CZA and (C) recalcined-CZA materials.

crystallinity. Consequently, the hydrothermal-like treatment gives rise to the hydrotalcite restoration as well as the growth of the CuO particles. When the latter sample is calcined (recalcined-CZA), the hydrotalcite decomposes into the corresponding metal oxides and, consequently, only CuO and ZnO peaks are detected. A high CuO crystallinity is maintained.

The mean crystalline sizes of CuO and ZnO for these materials were calculated using the Scherrer equation and are given in table 3. The CuO crystal size of the rehydrated CZA sample was higher by almost 40% than that of the base CZA sample. The fact that the crystallite size for the recalcined CZA material is similar to that of the rehydrated CZA clearly indicates that the increase of CuO crystallinity results from the hydrothermal-like treatment and not from the further recalcination. In parallel, the enhancement in the CuO particle size is accompanied by a decrease in the BET area (table 3).

When the latter results are compared with those of the Pd-modified samples, the similarity between the systems is evident. The average CuO particle size and BET area for the Pd-modified materials are very similar to those of the recalcined CZA sample. This finding leads us to conclude that the increase in the CuO crystallinity found for the modified Pd/CZA samples is caused by the hydrothermal-like treatment during the wet Pd impregnation step. In addition to the hydrotalcite reconstruction of the CuO–ZnO–Al_2O_3 composite oxide, a rearrangement of the CuO phase takes place that results in larger CuO crystallites.

In connection with the observation discussed above, several authors have already reported secondary phenomena during the hydrotalcite reconstruction in

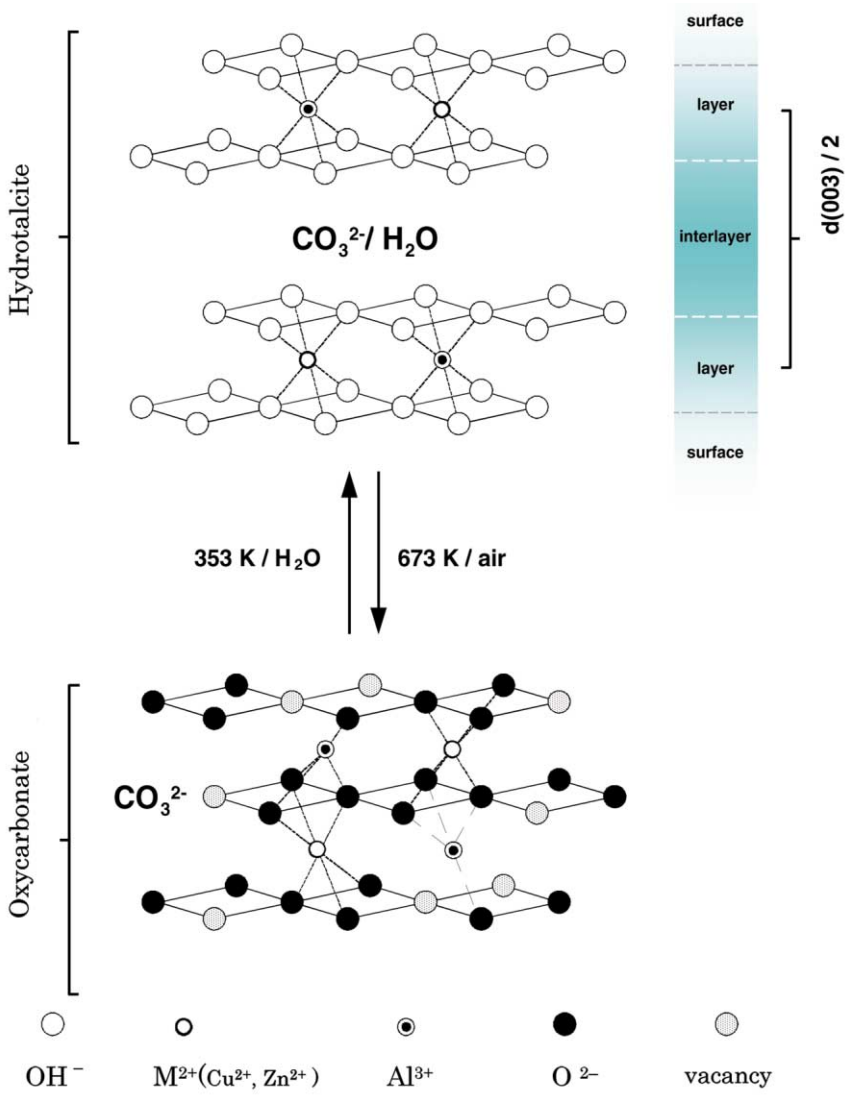

Figure 5. Representation model for the decomposition–reconstruction process of the parent HTCu–Zn hydrotalcite during a hydrothermal-like treatment.

mixed oxides. Kooli *et al.* [33] found an improvement in ZnO crystallinity during the rehydration of Zn–Al layered double hydroxides. Hibino and Tsunashima [13] demonstrated the segregation of aluminum from the structure upon performing calcination and reconstruction cycles on Mg–Al–CO_3 hydrotalcite. The same authors also reported an improvement in Mg–Fe spinel formation due to hydration/calcination cycles in Mg–Fe–CO_3 hydrotalcites [34]. In terms of our system, it can be suggested that the migration of water plays a key role in the CuO rearrangement process. The ability of water molecules to diffuse into the carbonate-modified CuO–ZnO–Al_2O_3 oxide and reconstruct the hydrotalcite would cause the growth of CuO crystallites by coalescence. Although a more detailed study is needed to confirm such a hypothesis and provide a definitive interpretation, this coalescence concept for copper oxide-containing materials has already been introduced [35] to explain the effect of the calcination heating rate on the CuO phase crystallinity for CuO–ZnO-based materials.

Table 3
BET specific area and CuO crystal size for CZA calcined sample and derived materials.

Sample	BET area (m^2/g)	XRD crystal size D_{CuO} (nm)
CZA	39.5	8.1
Rehydrated CZA	24.9	11.3
Recalcined CZA	33.6	11.3

4. Conclusions

We have shown that the carbonate anion retention in the calcined CZA starting material, which is due to incomplete Cu–Zn hydrotalcite decomposition, has important implications for the subsequent wet palladium

impregnation. The hydrothermal-like treatment of the carbonate-containing CZA oxide, during the Pd-impregnation step, allows the reconstruction of the Cu–Zn hydrotalcite-type structure. Such a regeneration process has a marked effect on the Pd-modified materials finally obtained. In particular, it results in the enhancement of the CuO phase crystallinity as a consequence of a crystalline rearrangement of this oxidic phase. The concept of coalescence between CuO crystallites, during the hydrotalcite restoration, is advanced as responsible for such increase of CuO crystallinity. This effect could have significant implications for the hydrogenation of CO_2 to methanol.

Acknowledgments

This work was supported by CICYT (Spain) under Grant QUI98-0877. I.M.C. thanks the Ministry of Education and Science for a fellowship.

References

[1] K. Klier, Adv. Catal. 31 (1982) 243.
[2] J.C.J. Bart and R.P.A. Sneeden, Catal. Today 2 (1987) 1.
[3] G.C. Chinchen, P.J. Denny, J.R. Jennings, M.S. Spencer and K.C. Waugh, Appl. Catal. 36 (1988) 1.
[4] F. Cavani, F. Trifirò and A. Vaccari, Catal. Today 11 (1991) 173.
[5] M. Saito, T. Fujitani, M. Takeuchi and T. Watanabe, Appl. Catal. A: General 138 (1996) 311.
[6] T. Inui, H. Hara, T. Takeguchi and J.B. Kim, Catal. Today 36 (1997) 25.
[7] T. Inui and T. Takeguchi, Catal. Today 10 (1991) 95.
[8] K. Fujimoto and Y. Yu, in: *New Aspects of Spillover Effect in Catalysis*, eds. T. Inui, *et al.* (Elsevier, Amsterdam, 1993) p. 393.
[9] M. Sahibzada, D. Chadwick and I.S. Metcalfe, Catal. Today 29 (1996) 367.
[10] I. Melián-Cabrera, M. López Granados, P. Terreros and J.L.G. Fierro, Catal. Today 45 (1998) 251.
[11] S. Miyata, Clays Clay Miner. 28 (1980) 50.
[12] T. Sato, K. Kato, T. Endo and M. Shimada, React. Solids 2 (1986) 253.
[13] T. Hibino and A. Tsunashima, Chem. Mater. 10 (1998) 4055.
[14] X-ray Powder Data File, JCPDS 38-487.
[15] X-ray Powder Data File, JCPDS 36-1475.
[16] P. Gherardi, O. Ruggeri, F. Trifirò, A. Vaccari, G. del Piero, G. Manara and B. Notari, in: *Preparation of Catalysts III*, eds. G. Poncelet, P. Grange and P.A. Jacobs (Elsevier, Amsterdam, 1983) p. 723.
[17] J.L. Li and T. Inui, Appl. Catal. A: General 137 (1996) 105.
[18] S. Miyata, Clays Clay Miner. 23 (1975) 369.
[19] W.T. Reichle, S.Y. Kang and D.S. Everhardt, J. Catal. 101 (1986) 352.
[20] T. Sato, H. Fujita, T. Endo, M. Shimada and A. Tsunashima, React. Solids 5 (1986) 219.
[21] M. Belloto, B. Rebours, O. Clause, J. Lynch, D. Bazin and E. Elkaïm, J. Phys. Chem. 100 (1996) 8527.
[22] M. del Arco, P. Malet, R. Trujillano and V. Rives, Chem. Mater. 3 (1999) 624.
[23] J. Pérez-Ramírez, G. Mul, F. Kapteijn and J.A. Moulijn, J. Mater. Chem. 11 (2001) 821.
[24] X-ray Powder Data File, JCPDS 80-1268.
[25] X-ray Powder Data File, JCPDS 38-487.
[26] L. Alejo, R. Lago, M.A. Peña and J.L.G. Fierro, Appl. Catal. 162 (1997) 281.
[27] R.T. Figueiredo, A. Martínez-Arias, M. López Granados and J.L.G. Fierro, J. Catal. 178 (1998) 146.
[28] D.O. Klenov, G.N. Kryukuva and L.M. Plyasova, J. Mater. Chem. 8 (1998) 1665.
[29] A.J. Marchi and C.R. Apesteguía, Appl. Clay Sci. 13 (1998) 35.
[30] J. Pérez-Ramírez, G. Mul, F. Kapteijn and J.A. Moulijn, Mater. Res. Bull. 36 (2001) 1767.
[31] F. Rey, V. Fornés and J.M. Rojo, J. Chem. Soc. Faraday Trans. 88 (1992) 2233.
[32] M. Belloto, B. Rebours, O. Clause, J. Lynch, D. Bazin and E. Elkaïm, J. Phys. Chem. 100 (1996) 8535.
[33] F. Kooli, C. Depège, A. Ennaqadi, A. de Roy and J.P. Besse, Clays Clay Miner. 45 (1997) 92.
[34] T. Hibino and A. Tsunashima, J. Mater. Sci. Lett. 19 (2000) 1403.
[35] S. Fujita, S. Moribe, Y. Kanamori, M. Kakudate and N. Takezawa, Appl. Catal. A: General 207 (2001) 121.